Clinical Kidney Journal, 2025, vol. 18, no. 3, sfaf040

https://doi.org/10.1093/ckj/sfaf040
Advance Access Publication Date: 8 February 2025
Original Article

ORIGINAL ARTICLE

Preoperative localization of parathyroid glands in secondary hyperparathyroidism: correlations between 99mTc-MIBI-SPECT/CT, ultrasound, and pathological characteristics

Binghan Li [1], Xiaoli Zhao [2,3], Sha Luo [4], Qi Zhong [5,6], Hanxue Zhao [7], Chengxiang Du [8] and Guojuan Zhang [1]

[1]Department of Nephrology, Beijing Tongren Hospital, Capital Medical University, Beijing, China, [2]Department of Pathology, Beijing Tongren Hospital, Capital Medical University, Beijing, China, [3]Beijing Key Laboratory of Head and Neck Molecular Diagnostic Pathology, Beijing Tongren Hospital, Capital Medical University, Beijing, China, [4]Department of Nuclear Medicine, Beijing Tongren Hospital, Capital Medical University, Beijing, China, [5]Department of Otorhinolaryngology – Head and Neck Surgery, Beijing Tongren Hospital, Capital Medical University, Beijing, China, [6]Key Laboratory of Otolaryngology – Head and Neck Surgery (Capital Medical University), Ministry of Education, Beijing, China, [7]Department of Diagnostic Ultrasound, Beijing Tongren Hospital, Capital Medical University, Beijing, China and [8]Emory University Rollins School of Public Health, Atlanta, GA, USA

Correspondence to: Guojuan Zhang; E-mail: guojuanzhang520@126.com

ABSTRACT

Objective. To investigate the association between imaging findings and histopathological characteristics of parathyroid glands in patients with secondary hyperparathyroidism (SHPT).

Methods. Seventy-four glands from 21 patients with SHPT who underwent parathyroidectomy were evaluated for their pathological characteristics. The detection rates of parathyroid glands using ultrasound (US) and 99Tc-MIBI-SPECT/CT (MIBI) were compared. Glands were classified as either US-positive or US-negative, and MIBI-positive or MIBI-negative. Morphological and pathological differences between the positive and negative groups were systematically analysed.

Results. The detection rates for parathyroid glands were 71% with US, 65% with MIBI, and 82% when combining both methods. US and MIBI showed similar localization accuracy in SHPT ($P = .38$). MIBI-positive glands had significantly larger oxyphil nodules compared with MIBI-negative glands (area: 10.92 mm² vs 3.09 mm², $P < .01$; area proportion: 61% vs 30%, $P = .002$), while no significant differences were found in chief nodules. The US-positive group had fewer and smaller chief nodules (number: 2 vs 9, $P = .005$; area: 1.53 mm² vs 11.08 mm², $P = .033$) and a higher percentage of oxyphil nodules (74% vs 33%, $P = .003$) compared with the US-negative group. Thirteen glands undetected by both US and MIBI had smaller oxyphil nodule areas (3.59 vs 13.24 mm²) and lower oxyphil nodule area percentages (25% vs 68%). These pathological features, including adipose infiltration, intra-gland haemorrhage, cyst formation, and calcification, showed no correlation with the gland's imaging results.

Received: 13.9.2024; Editorial decision: 31.1.2025

Conclusion. US and MIBI had similar value in preoperative localization of SHPT. Parathyroid glands with more and larger oxyphil nodules were more likely to be detected by both MIBI and US.

Keywords: 99Tc-MIBI-SPECT/CT, chief cell, oxyphil cell, secondary hyperparathyroidism, ultrasound

KEY LEARNING POINTS

What was known:

- Parathyroidectomy is a crucial surgical treatment for secondary hyperparathyroidism (SHPT).
- Preoperative ultrasound (US) and 99Tc-MIBI-SPECT/CT (MIBI) determine the effectiveness of parathyroidectomy, but neither can locate all the parathyroid glands.
- SHPT is characterized by increased oxyphil cell content, nodular proliferation, adipose infiltration, intraglandular haemorrhage, calcification, and fluid-cyst formation.

This study adds:

- The pathological characteristics of parathyroid glands are correlated with the detection rate of US and MIBI.
- Adipose infiltration, intraglandular haemorrhage, calcification, and fluid-cysts do not impact imaging results.
- Parathyroid glands with more and larger oxyphil nodules are more likely to be detected by US and MIBI.

Potential impact:

- The study further supports the idea that oxyphil cells may play an important role in SHPT.
- US and MIBI can be used clinically as markers to detect the progression of SHPT to advanced stages based on the increasing number and volume of oxyphil nodules.

INTRODUCTION

Chronic kidney disease–mineral bone disorder (CKD–MBD) is characterized by dysregulated calcium and phosphorus metabolism, in addition to alterations in parathyroid hormone (PTH) levels and fibroblast growth factor 23 (FGF-23), thereby contributing to vascular calcification and heightened cardiovascular risk [1]. The pathophysiological mechanism of CKD–MBD is primarily attributed to secondary hyperparathyroidism (SHPT), which is characterized by parathyroid gland hyperplasia and excessive PTH secretion. SHPT is a significant prognostic risk factor in patients with CKD, necessitating aggressive management strategies to attain target PTH levels and to optimize patient outcomes [2]. In certain cases, despite comprehensive drug therapy, the parathyroid gland may persistently proliferate alongside continuous increases in PTH levels. In such circumstances, surgical excision of hyperplastic parathyroid glands is often necessary [3].

In contrast to primary hyperparathyroidism (PHPT), the surgical management of SHPT often necessitates the complete excision of all identifiable parathyroid tissue due to potential stimulation by various factors, such as elevated phosphorus levels, which can lead to SHPT recurrence [4]. Therefore, preoperative imaging techniques for the accurate localization of parathyroid tissue in SHPT patients present greater challenges than those employed in PHPT patients. Ultrasound (US) and 99mTc-MIBI-SPECT (MIBI) are the most frequently utilized non-invasive examinations in clinical practice. However, neither of these methods can effectively detect all potential parathyroid glands. The accuracy of US and MIBI imaging for detecting parathyroid glands is influenced by various factors; however, existing studies have focused primarily on PHPT involving parathyroid adenoma or carcinoma rather than on SHPT [5–8]. Therefore, an investigation of the characteristics of and factors influencing parathyroid US and MIBI in the localization of SHPT holds significant scientific and clinical value.

Compared with PHPT, SHPT has distinct pathological features. Under normal physiological conditions, the parathyroid gland consists mainly of chief cells, which are responsible for PTH secretion, along with sporadic oxyphilic cells, whose function remains unknown. However, in SHPT there is a significant deviation from this state. During the early stages of SHPT, there is diffuse proliferation of glandular cells, which subsequently give rise to fibrous nodules as the disease progresses [9, 10]. This progression is accompanied by the development of fluid-filled cysts, tissue calcification, infiltration of adipose tissue, and intraglandular haemorrhage. Notably, oxyphil cell proliferation becomes particularly prominent in SHPT and may even lead to the formation of giant oxyphil nodules—a characteristic pathological manifestation unique to this condition. Furthermore, the precise role of chief cells and oxyphil cells in SHPT remains elusive. The cytoplasm of oxyphil cells is predominantly occupied by dysfunctional mitochondria, suggesting a potential absence of endocrine functions. However, numerous studies have demonstrated that, compared with chief cells, oxyphil cells exhibit an even greater capacity for synthesizing PTH [11]. Investigating the pathological characteristics of SHPT serves as a crucial starting point for exploring its pathogenesis.

Given the distinct morphological and functional differences between chief cells and oxyphil cells, their appearance on imaging may vary. Consequently, parathyroid glands with varying cell compositions can exhibit diverse characteristics in US and nuclear medicine evaluations. To investigate the pathological characteristics of the parathyroid glands on imaging and to identify potential factors that may influence the US and MIBI results from a pathological perspective, we conducted a correlation analysis between pathology and imaging examinations of 74 parathyroid tissues obtained from 21 patients with SHPT.

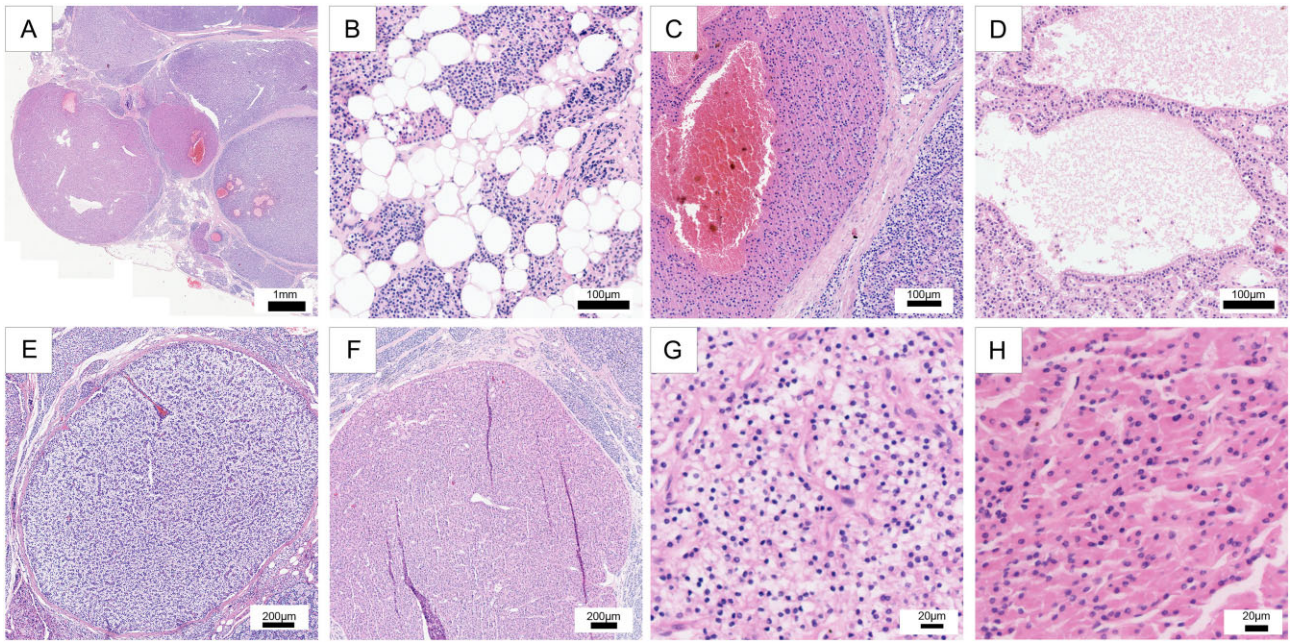

Figure 1: Pathological characteristics of SHPT. The parathyroid glands of patients with SHPT were surgically removed and stained with H&E. The merged field of view revealed nodular hyperplasia in the gland (**A**). Histological examination also showed fat infiltration (**B**), intraglandular haemorrhage (**C**), and formation of fluid-filled cystic cavities within the tissues (**D**). The chief cells and oxyphilic cells were surrounded by fibrous tissue, forming chief cell nodules (**E**) and oxyphilic cell nodules (**F**). Upon H&E staining, the cytoplasm of the chief cells appeared lightly stained with small-sized cell bodies (**G**), while the cytoplasm of the oxyphilic cells showed strong eosinophilia with relatively larger cell bodies (**H**).

MATERIALS AND METHODS

Subjects

This was a single-institution retrospective study. Between January 2017 and March 2021, 21 consecutive uremic patients (11 male, 10 female, 20 who received haemodialysis, and 1 who received peritoneal dialysis) with biochemically suggestive SHPT underwent parathyroidectomies. According to the KDIGO 2017 Clinical Practice Guidelines [11], all patients were diagnosed with SHPT and met the criteria for parathyroidectomy. Briefly, patients with CKD stage 5D with severe hyperparathyroidism (over 9 times the upper normal limit) who failed to respond to pharmacological therapy were considered suitable for parathyroidectomy. Thirteen patients exhibited resistance to all available treatments, including calcium supplements, phosphate binders, calcitriol, and calcimimetics, indicating a potential progression to tertiary hyperparathyroidism. Eight patients were unable to receive calcimimetics due to severe adverse reactions or drug unavailability, which hindered a definitive assessment of PTH responsiveness. Consequently, all subjects in this study were classified as having SHPT. Patient records were carefully reviewed, and clinical information, including body mass index (BMI), dialysis vintage, underlying disease, and medication history, was collected.

Laboratory parameters

Full-length PTH levels were measured preoperatively and 1 day postoperatively using a second-generation assay on a Beckman Coulter CX4CE automatic biochemical analyser (Beckman Coulter, USA). Alkaline phosphatase (ALP) levels, with a normal reference range of 50–35 U/L, were determined by continuous monitoring colorimetry using the same instrument. Additionally, other routine serum biochemical indicators were assessed for all patients included in the study: total calcium (2.20–2.65 mmol/L), phosphate (0.9–1.6 mmol/L), alanine aminotransferase (ALT) (7–40 U/L), aspartate aminotransferase (AST) (13–35 U/L), urea (3.1–8.8 mmol/L), and creatinine (41–81μ mol/L). Both US and MIBI examinations were conducted preoperatively to facilitate precise localization of the parathyroid glands in all patients. During surgery, all accessible parathyroid tissue was removed while the plasma PTH levels were continuously monitored. The operation was deemed successful when a reduction of $>$70% in PTH levels compared with preoperative values was achieved, along with complete excision of all identifiable parathyroid glands.

Parathyroid tissue preparation and haematoxylin–eosin staining

The surgical procedure was a total parathyroidectomy under general anaesthesia, involving the removal of all identifiable parathyroid glands without forearm subcutaneous transplantation. In brief, the steps were: (i) a transverse neck incision exposed and excised both normal and ectopic parathyroid glands, with tissues sent for frozen section analysis; (ii) PTH levels were measured in blood samples; (iii) if fewer than four glands were found or PTH levels remained $\geq$400 pg/mL, exploration extended to retro-oesophageal, deep paratracheal spaces, the substernal region, the carotid sheath, the thyroid gland, and the thymus to locate and remove any missed glands; (iv) success was confirmed by an 80% drop in PTH levels from preoperative values.

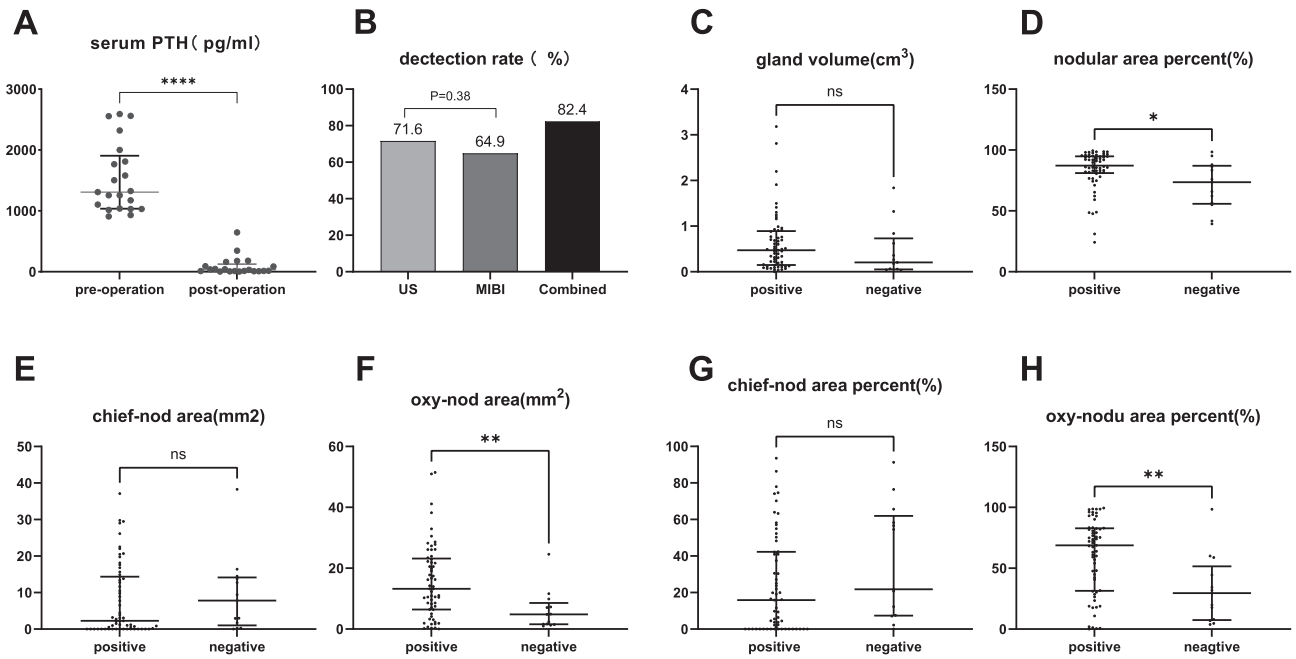

Figure 2: Serum PTH levels, detection rate, and parathyroid characteristics in combined positive vs negative groups. (**A**) Serum PTH levels before and 1 day post-operation. (**B**) Overall detection rate of the parathyroid gland by ultrasound (US), 99mTc-MIBI-SPECT/CT (MIBI), and combined (US + MIBI) imaging. (**C–H**) Characteristics of the combined positive group ($n = 61$) vs the negative group ($n = 13$). Each point represents an individual gland's measurement, while the lines show the median and interquartile range. (**C**) Parathyroid gland volume. (**D**) Percentage of nodular area. (**E**) Area of the chief nodule. (**F**) Area of the oxyphil nodule. (**G**) Percentage of chief nodule area. (**H**) Percentage of oxyphil nodule area. ns, no statistical difference; *$P < .05$; **$P < .01$; ****$P < .0001$.

A total of 74 parathyroid glands were surgically excised from 21 patients. Subsequently, precise measurements of length, width, and height were promptly obtained using a Vernier calliper. The volume of the hyperplastic parathyroid lesion was estimated following previously established methodologies [12]. Briefly, the volume was calculated using the formula $V = 4/3\pi(abc)$, where V represents the volume of each parathyroid lesion determined by its three radii (a, b, and c). The glands were subsequently fixed in 4% formalin, embedded in paraffin and sectioned into 4-μm thick slices. These sections were uniformly stained with haematoxylin and eosin (H&E). Two experienced pathologists independently evaluated the H&E-stained sections. Among the 74 surgically removed tissues, both pathologists consistently diagnosed all samples as secondary hyperplastic parathyroid glands. Related H&E-stained slices, which were meticulously selected from the largest cross-sectional area of each gland, were subsequently selected for further quantitative analysis in the field of pathology.

Histological image acquisition and analysis

The parathyroid slices stained with H&E were scanned using the TissueFAX platform (TissueGnostics, Vienna, Austria) at a magnification of 20× and merged into a combined image for each gland. Further quantitative analysis was performed on these images using StrataQuest software (version 7.0, TissueGnostics, Vienna, Austria). By employing the colour separation engine of StrataQuest, oxyphil cells, characterized by intense eosinophilia in their cytoplasm, were automatically distinguished from chief cells via subtle staining. The number, cell count, area, and cell density of oxyphil nodules and chief nodules (defined as oxyphil or chief cells surrounded by fibrous tissue) were subsequently assessed. The presence of fatty infiltration, cysts, calcifications, and haemorrhages was also documented (Fig. 1).

Imaging protocols

A dual-phase 99mTc-MIBI SPECT/CT scan was performed as a routine procedure in all patients. SPECT/CT images of the cervical region and thorax were acquired 15 minutes (early stage) and 120 minutes (late stage) after intravenous administration of 555 MBq of 99mTc-MIBI (HTA Co. Ltd, China). For image acquisition, a Discovery NM/CT 670 Pro system (GE Healthcare, Haifa, Israel) equipped with both parallel hole and pinhole high-resolution collimators was utilized. For the analysis of dual-phase imaging, a comparison was made between early and delayed 99mTc-MIBI planar images; regional uptake of 99mTc-MIBI with slower washout than that from thyroid tissue was considered indicative of hyperfunctioning parathyroid tissue.

Cervical ultrasound was performed on each patient using an iU22 high-resolution ultrasonic diagnostic device (Philips, Amsterdam, Netherlands) by an experienced radiologist to identify any proliferating parathyroid glands. A high-frequency linear transducer (5-12 MHz) was utilized to examine the region extending from the angles of the mandible to the sternal notch, with specific emphasis on the posterior thyroid gland, para- and retro-oesophageal space, carotid sheath, and retrosternal space. The parathyroid gland, which appears hyperechoic on ultrasound imaging, exhibits distinct demarcation from the surrounding thyroid parenchyma and demonstrated dynamic movement during swallowing, showing robust vascular supply. The number, size, location, echogenicity, and morphology of the parathyroid glands were meticulously documented.

Statistical analysis

Descriptive statistics were employed based on the data type: categorical variables were analysed using frequencies and corresponding percentages, while continuous variables were initially assessed for normality and are presented as the mean ± standard deviation if they followed a normal distribution; otherwise, the median and range are reported. The difference between the negative and positive groups of imaging examinations (MIBI+ vs MIBI−, US+ vs US−) was analysed. If the data were continuous, a *t*-test was used; for categorical data, a χ^2 test was used. In the analysis comparing the detection rates of parathyroid glands between US and MIBI, appropriate statistical tests were employed based on the type of data. These tests included paired *t*-tests, McNemar tests, and standard χ^2 tests. In particular, mid-*P* McNemar's test was utilized when inconsistent sample size was small [13]. Statistical analysis was performed using IBM SPSS Statistics 26.0 for Windows (Chicago, IL, USA). *P* values <.05 were considered to indicate statistical significance.

RESULTS

Patient information

Clinical information from 21 patients with stage 5 CKD undergoing dialysis was collected and analysed, along with pathological and imaging information obtained from 74 excised parathyroid glands. The median dialysis vintage of 20 haemodialysis patients (4 hours per session, 3 times per week) and 1 peritoneal dialysis patient (10 litres per day) was 96 months. Thirteen patients received cinacalcet therapy, while eight patients were unable to tolerate or access cinacalcet. Despite appropriate pharmacotherapy, there was persistent uncontrolled and significant elevation in PTH levels (with a median value of 1309 pg/mL), accompanied by parathyroid gland enlargement. After surgery, a significant reduction in PTH concentration was observed in 21 patients, with a median blood PTH concentration of 32.2 pg/mL on the first postoperative day (Fig. 2A). Nine patients underwent removal of fewer than four parathyroid glands, 11 patients underwent removal of exactly four parathyroid glands, and one patient underwent removal of more than four parathyroid glands. In total, a total of 74 parathyroid glands were surgically excised. Additionally, an extensive analysis was conducted on the findings regarding the pathological characteristics and preoperative imaging associated with these 74 glands (Table 1).

Table 1: Characteristics of SHPT patients ($n = 21$).

Characteristics	Data
Age (years)	54.3 ± 8.5
Sex	
Male	11 (52%)
Female	10 (48%)
BMI (kg/m^2)	25.3 ± 3.8
Dialysis modality	
Haemodialysis	20(95%)
Peritoneal dialysis	1 (5%)
Dialysis vintage (months)	96 (36, 192)
Concomitant diseases	
Hypertension	19 (91%)
Diabetes mellitus	5 (24%)
Coronary heart disease	5 (24%)
Cerebrovascular disease	3 (14%)
Obstructive sleep apnoea syndrome	2 (10%)
Digestive ulcer	5 (24%)
Number of parathyroid glands removed	
<4	9 (43%)
4	11 (52%)
>4	1 (4.8%)
Preoperative PTH (pg/mL)	1309 (909, 2590)
Postoperative PTH (pg/mL)	32.2 (3.78, 646)
Preoperative correction calcium (mmol/L)	2.4 ± 0.2
Preoperative phosphorus (mmol/L)	2.5 ± 0.6
Preoperative ALP (mmol/L)	171 (92 697)
Preoperative predialysis urea (mmol/L)	21.1 ± 7.2
Preoperative predialysis creatinine (μmol/L)	771 ± 239.8
Preoperative haemoglobin (g/L)	115 (88, 164)
Preoperative ALT (U/L)	9.4 ± 5.3
Preoperative AST (U/L)	10.4 ± 3.0
Preoperative triacylglycerol (mmol/L)	1.82 (0.6, 5.47)
Preoperative total cholesterol (mmol/L)	4.1 ± 0.9
Medication history	
Phosphorus binding agent	21 (100%)
1,25-vitamin D3	21 (100%)
Cinacalcet	13 (63%)

Measurement data with a normal distribution are presented as mean ± standard deviation, while non-normal data are reported as median (minimum, maximum). Enumeration data are presented as frequencies and proportions.

Comparison between US and MIBI

To compare the efficacy of both imaging modalities for the preoperative localization of parathyroid glands, we evaluated the detection rate across various gland locations, sizes, and pathological characteristics. The US technique achieved an overall detection rate of parathyroid glands of 72% (53 out of 74), while the utilization of MIBI yielded a detection rate of 65% (48 out of 74). There was no statistically significant difference between the two groups ($P = .38$) (Table 2, Fig. 2B). The subgroup analysis revealed that for glands smaller than 0.5 cm^3, cervical US demonstrated a significantly greater detection rate (71%) than MIBI (50%, $P = .04$) for glands smaller than 0.5 cm^3. Both US and MIBI exhibited comparable efficacy in localizing parathyroid glands at different locations, irrespective of size or the presence of adipose tissue, calcification, cysts, or haemorrhage (Fig. 1), while also accommodating variations in oxyphil cell content. Additionally, the performance of US and 99mTc-MIBI-SPECT remained consistent regardless of the preoperative PTH level and prior cinacalcet medication (Table 3).

Table 2: Detection of parathyroid in SHPT by ultrasound and 99mTc-MIBI-SPECT/CT.

	99mTc-MIBI-SPECT/CT		
Ultrasound	+	−	Total
+	40	13	53
−	8	13	21
Total	48	26	74

The table shows the counts of parathyroid glands with different examination results from two imaging methods. '+' indicates glands detectable via ultrasound or 99mTc-MIBI-SPECT/CT imaging, while '−' means undetectable in preoperative examinations.

Table 3: Characteristics of 74 parathyroid lesions and overall performance of ultrasound (US) and 99mTc-MIBI-SPECT/CT (MIBI).

	N	US-positive	MIBI-positive	P value
Overall lesion	74	53 (72%)	48 (65%)	.38
Position				
Upper left	14	11 (79%)	7 (50%)	.13
Lower left	21	16 (76%)	15 (71%)	.63
Upper right	15	9 (60%)	6 (40%)	.22
Lower right	20	16 (80%)	17 (85%)	.69
Ectopia	4	1 (25%)	3 (75%)	.25
Volume (cm^3) 0.426 (0.002, 3.183)				
<0.5	42	30 (71%)	21 (50%)	.04
0.5–1.0	20	16 (80%)	17 (85%)	.62
>1.0	12	7 (58%)	10 (83%)	.13
Cinacalcet treatment				
Yes	50 lesions from 13 patients	36 (72%)	31 (62%)	.30
No	24 lesions from 8 patients	17 (71%)	17 (71%)	.69
Preoperative PTH (pg/mL)				
≥1500	35 lesions from 9 patients	24 (69%)	20 (57%)	.42
<1500	39 lesions from 12 patients	29 (74%)	28 (72%)	.73
Adipose infiltration				
Yes	26	21 (81%)	17 (65%)	.29
No	48	32 (67%)	31 (65%)	.79
Haemorrhage				
Yes	18	13 (72%)	12 (67%)	.69
No	56	40 (71%)	36 (64%)	.45
Cyst formation				
Yes	16	13 (81%)	12 (75%)	.69
No	58	40 (69%)	36 (62%)	.45
Calcification				
Yes	7	4 (57%)	6 (85%)	.38
No	67	49 (73%)	42 (62%)	.14
The area ratio of oxyphil nodules				
≥50%	43	36 (84%)	34 (79%)	.75
<50%	31	17 (55%)	14 (45%)	.55

Data are presented as the number of parathyroid glands that tested positive on either US or MIBI, along with their respective detection rates (%).
A statistically significant difference in the detection rate was defined as a P value <.05.

Correlation between MIBI results and pathological characteristics

The parathyroid glands ($n = 74$) were categorized into two groups based on the performance of MIBI imaging: a positive group (MIBI+, $n = 48$) and a negative group (MIBI−, $n = 26$). Subsequently, a comparative analysis was conducted to assess the characteristics of these two groups. The maximum cross-sectional area of the gland in the MIBI+ group (23.58 mm^2) was larger than that in the MIBI− group (17.89 mm^2), although there was no statistically significant difference in gland volume between the two groups. Compared with those in the MIBI− group, the MIBI+ group had significantly greater numbers of total parathyroid pathological cells (30.32×10^4 vs 26.90×10^4, $P < .001$) and nodular cells (24.56×10^4 vs 20.33×10^4, $P < .001$). To investigate the correlation between these two types of nodules and the MIBI results, we quantified the number, area, and proportion of oxyphil and chief cell nodules while comparing differences in these pathological characteristics between both groups of glands. A significantly greater median area of oxyphil nodules (10.92 vs 3.09 mm^2, $P < .01$) and a greater proportion of oxyphil nodules (61% vs 30%, $P = .002$) were detected in the MIBI+ group than in the MIBI− group. In contrast to those of oxyphil nodules, the number, area, and proportion of chief cell nodules did not significantly differ between the two groups. Moreover, there were no statistically significant differences in the occurrence of fat infiltration, calcification, intraglandular haemorrhage, or fluid cyst formation between the two groups (Table 4).

Correlation between US results and pathological characteristics

According to the results of the cervical US examinations, 74 glands were divided into two groups: a positive group (US+ group, $n = 53$) and a negative group (US− group, $n = 21$). To investigate correlations between pathological characteristics and the US detection rate, further comparisons and analyses were conducted on the characteristics of parathyroid glands in both the US+ and US− groups (Table 5). The proportion of nodule area in the US+ group was 86%, which was significantly greater than that in the US− group (85%, $P = .03$), despite the absence of any observed difference in gland volume between these two groups ($P = .81$). Notably, there was a significantly greater number of chief nodules in the US− group than in the US+ group (mean difference = 4, 95% CI: 1–6, $P = .005$). Similarly, the area of the parathyroid chief nodule in the US− group was significantly larger than that in the US+ group (11.08 vs 1.53, $P = .03$). Notably,

Table 4: Comparison of pathological characteristics in parathyroid glands between MIBI-positive and MIBI-negative group.

	MIBI+ (N = 48)	MIBI− (N = 26)	P value
Overall characteristics			
Volume (cm^3)	0.43 (0.12, 0.85)	0.20 (0.07, 0.49)	.02
Total area (mm^2)	23.58 (16.01, 38.97)	17.89 (10.21, 24.08)	.003
Percentage of nodular area	86 (76.22, 94.63)	81.81 (55.86, 92.95)	.02
Total cell count ($\times 10^4$)	30.32 (18.95, 49.20)	26.90 (12.52, 34.62)	.02
Nodular cell count ($\times 10^4$)	24.56 (16.56, 39.30)	20.33 (10.77, 26.57)	<.001
Non-nodular cell count ($\times 10^4$)	2.97 (1.00, 9.84)	3.55 (1.06, 10.42)	.57
Total cell density ($\times 10^3/mm^2$)	12.83 (10.77, 14.73)	12.91 (11.28, 15.22)	.43
Nodular cell density ($\times 10^3/mm^2$)	12.78 (10.17, 15.26)	13.05 (10.99, 15.59)	.54
Non-nodular cell density ($\times 10^3/mm^2$)	9.94 (5.67, 14.07)	12.33 (7.53, 18.19)	.39
With fat	17 (35%)	9 (35%)	.95
With calcification	6 (13%)	1 (4%)	.41
With haemorrhage	12 (25%)	6 (23%)	.85
With cyst	12 (25%)	4 (15%)	.34
Characteristics of oxyphil nodules			
Number of oxyphil nodules	6 (2, 9)	6 (5, 9)	.21
Area of oxyphil nodules (mm^2)	10.92 (3.71, 22.05)	3.09 (1.66, 10.08)	<.001
Percentage of oxyphil nodule area	61.00 (27.44, 81.92)	30.29 (12.79, 68.71)	.002
Characteristics of chief nodules			
Number of chief nodules	3 (0, 9)	4 (1, 9)	.55
Area of chief nodules (mm^2)	2.97 (0, 14.14)	3.17 (1.14, 13.29)	.97
Percentage of chief nodule area	16.51 (0, 51.31)	30.55 (7.34, 57.73)	.06

MIBI, 99mTc-MIBI-SPECT/CT.
Measurement data are reported as median (interquartile range) and enumeration data as frequencies and proportions.
A statistically significant difference in the detection rate was defined as a *P* value <.05.

there was a considerably greater proportion of oxyphil nodules in the US+ group than in the US− group (74% vs 33%, $P = .003$). Moreover, the incidence of fat encapsulation, occurrence of calcification, presence of haemorrhage, and frequency of fluid cyst formation did not exhibit any notable differences between the two groups. These findings align with the results obtained from MIBI analysis.

Correlation between combined US and MIBI detection rates and parathyroid characteristics

In clinical practice, US and MIBI imaging are frequently used concurrently for preoperative localization of parathyroid glands. A statistical analysis was conducted on the combined detection rate of 74 parathyroid glands using US and MIBI. Of these 74 glands, 61 were successfully identified by the combination of US and MIBI, resulting in a combined detection rate of 82% (Fig. 2B). Thirteen glands remained undetected by both modalities prior to surgery. Compared with the positive group, the 13 undetected glands exhibited significantly lower percentages of hyperplastic nodules, oxyphilic nodule areas, and oxyphilic nodule area proportions. However, there were no statistically significant differences in gland volume, chief cell nodule area, or chief cell nodule area proportion (Fig. 2C–H, Supplementary Table S1).

DISCUSSION

US and MIBI are the most widely used examinations for preoperative localization; however, their results can be influenced by various factors. In this study, a total of 74 parathyroid glands were selected to investigate the correlation between their pathological characteristics and imaging findings. The results indicated that US and MIBI had similar localization values for the parathyroid gland in SHPT patients (detection rate: 71% vs 65%). However, according to the data of Ishii and colleagues, US detection of parathyroid glands in SHPT patients was significantly greater than that in MIBI patients (93% vs 61%) [8]. The difference between that study and the current one may be attributed to differences in the study population. Specifically, patients with both primary and secondary hyperparathyroidism, only eight of whom were patients with SHPT, and only 32 parathyroid glands were included in the previous study. Additionally, several factors may have influenced the imaging findings, such as the location and size of the gland, the presence of a parathyroid cyst, and the use of cinacalcet treatment [8, 14, 15]. These factors could explain the wide variability observed in US and MIBI detection rates across different studies.

In the present study, although the number of oxyphil nodules remained consistent, the area occupied by oxyphil nodules was significantly greater in the MIBI+ group. A similar phenomenon has also been documented in patients with primary parathyroid hyperplasia and parathyroid adenoma [16]. The specific mechanism of 99mTc-MIBI uptake by the parathyroid gland remains unclear. However, *in vitro* cell experiments have confirmed a potential close association between 99mTc-MIBI uptake and mitochondrial membrane function [17]. Importantly, SHPT results in an abundance of oxyphil cells filled with numerous mitochondria [18], which may explain the correlation between the oxyphil cell content and MIBI results.

The appearance of the parathyroid glands on US can be attributed to their cellular composition. Glands with a hypoechoic appearance are likely to have a greater abundance of functional cells, while isoechoic or hyperechoic glands may contain a greater proportion of non-functional components [19]. However, the presence of non-functional components such as fatty tissue, calcification, cysts, and haemorrhage did not appear to affect the results of US imaging in the present study. In this study, US demonstrated a higher detection rate of 71% for parathyroid

Table 5: Comparison of pathological characteristics in parathyroid glands between ultrasound (US)-positive and US-negative groups.

	US+ (N = 53)	US− (N = 21)	P value
Overall characteristics			
Volume (cm^3)	0.45 (0.15, 0.82)	0.27 (0.07, 1.07)	.81
Total area (mm^2)	23.94 (16.44, 35.02)	22.76 (15.66, 49.11)	.07
Percentage of nodular area	86.00 (81.10, 95.26)	84.79 (55.45, 92.69)	.03
Total cell count ($\times 10^4$)	28.49 (18.42, 46.46)	33.24 (22.45, 62.91)	.06
Nodular cell count ($\times 10^4$)	24.56 (16.61, 39.56)	24.88 (13.54, 39.29)	.80
Non-nodular cell count ($\times 10^4$)	2.48 (0.55, 5.44)	8.02 (1.84, 18.64)	.03
Total cell density ($\times 10^3/mm^2$)	12.53 (10.05, 14.73)	13.14 (11.11, 15.49)	.20
Nodular cell density ($\times 10^3/mm^2$)	12.87 (10.17, 15.07)	12.29 (10.19, 16.75)	.68
Non-nodular cell density ($\times 10^3/mm^2$)	9.37 (5.08, 12.92)	14.07 (0.76, 30.23)	.03
With fat	21 (40%)	5 (24%)	.28
With calcification	4 (8%)	3 (14%)	.40
With haemorrhage	13 (25%)	5 (24%)	.95
With cyst	13 (25%)	3 (14%)	.53
Characteristics of oxyphil nodules			
Number of oxyphil nodules	6 (1, 8)	7 (5, 10)	.11
Area of oxyphil nodules (mm^2)	13.22 (5.71, 22.59)	7.39 (1.63, 17.39)	.34
Percentage of oxyphil nodule area	73.74 (31.41, 83.37)	33.02 (10.37, 62.65)	.003
Characteristics of chief nodules			
Number of chief nodules	2 (0, 6)	9 (4, 11)	.005
Area of chief nodules (mm^2)	1.53 (0, 12.23)	11.08 (2.93, 16.20)	.03
Percentage of chief nodule area	9.38 (0, 42.28)	22.74 (14.00, 63.81)	.06

Measurement data are reported as median (interquartile range) and enumeration data as frequencies and proportions.
A statistically significant difference in the detection rate was defined as a *P* value <.05.

glands with a volume <0.5 cm^3. This may be attributed to the relatively lower spatial resolution of MIBI-SPECT, which limits its ability to accurately identify smaller glands. Consequently, US appears to be a more effective tool for screening and monitoring SHPT, allowing earlier detection of parathyroid gland enlargement. The US+ group exhibited a greater prevalence of larger oxyphil nodules, suggesting that glands with more oxyphil content may be more easily detected by US. This observation aligns with previous studies on PHPT [20]. Recent studies confirmed that PTH expression levels in oxyphilic cells are significantly greater than those in chief cells [21]. The correlation between oxyphil cell content and findings obtained via ultrasound imaging may further support the potential role of oxyphil cells in SHPT.

In the current study, a higher content of oxyphil cells was associated with easier detection by MIBI and US examination. These findings have several clinical implications. First, previous studies have suggested that oxyphilic cells may play a role in SHPT, and the correlation between the cell composition of the parathyroid gland and imaging findings further confirms this speculation. Second, during the progressive course of SHPT, there is dynamic evolution in the cellular components of parathyroid glands, transitioning from diffuse hyperplasia with lower oxyphil contents in the early stages to an increased presence of oxyphil cells with nodule formation in the later stages [22]. The association between imaging results and cell composition suggests that imaging techniques could be used to monitor disease progression and medication response. Indeed, studies have demonstrated that US and MIBI can be utilized to monitor therapeutic responsiveness to cinacalcet treatment as well as outcomes following kidney transplantation for SHPT patients [14, 23]. The study found that both US and MIBI are equally effective in detecting parathyroid glands in SHPT. Glands with severe nodular hyperplasia and a high proportion of oxyphil nodules are more likely to be detected. As this pathological feature becomes progressively more pronounced with the advancement of SHPT, US and MIBI may serve as effective tools for assessing the disease stage of SHPT in clinical settings, thereby aiding in surgical decision-making.

This study also has several limitations. On one hand, the sample size was relatively small. Some obvious differences, such as the difference in the ability to detect ectopic parathyroid glands between MIBI and US, were not statistically significant. On the other hand, the pathological section of the largest cross-section of the gland was selected to represent the pathological situation of the whole gland in this study. However, the pathological characteristics of such a section may not completely reflect the situation of the whole gland, especially some relatively small nodules, which may not be reflected in the section. The value of other non-invasive examination methods, such as CT, positron emission tomography (PET), and enhanced US, needs to be further explored and applied in cases of SHPT [14, 24–27].

SUPPLEMENTARY DATA

Supplementary data are available at *Clinical Kidney Journal* online.

ACKNOWLEDGEMENTS

The Department of Otorhinolaryngology and Head and Neck Surgery, Beijing Tongren Hospital, is acknowledged for their superb surgery and the provision of general information related to the parathyroid gland. The Department of Pathology, Nuclear Medicine and Diagnostic Ultrasound is acknowledged for providing pathological slides and images related to the parathyroid.

FUNDING

The research was financially supported by the Beijing Natural Science Foundation (No. 7212021). However, the funding source played no role in the study's design and execution, data analysis and interpretation, or manuscript preparation, review, and approval.

AUTHORS' CONTRIBUTIONS

Guarantor of integrity of the entire study: G.Z. Study concepts and design: B.L., G.Z. Literature research: B.L., G.Z., C.D. Experimental studies/data analysis: X.Z., S.L., Q.Z., H.Z. Statistical analysis: C.D., B.L. Manuscript preparation: BL., G.Z. Manuscript editing: G.Z.

AUTHOR DECLARATION

The content, title, and authorship order of this article have received unanimous approval from all authors. The Author's Declaration Form has been signed by all authors and submitted alongside the manuscript.

CONFLICT OF INTEREST STATEMENT

The authors declare no conflict of interest.

DATA AVAILABILITY STATEMENT

The datasets utilized in this study can be obtained from the corresponding author upon reasonable request.

ETHICS APPROVAL

The present study has obtained approval from the Ethics Committee on Human Research at Tongren Hospital, Capital Medical University. All clinical data and parathyroid images were collected with the granted approval of the committee. The data were obtained during routine patient care. After a thorough review, the ethics committee granted a waiver for informed consent.

REFERENCES

1. Cannata-Andía JB, Martín-Carro B, Martín-Vírgala J *et al*. Chronic kidney disease-mineral and bone disorders: pathogenesis and management. *Calcif Tissue Int* 2021;**108**:410–22. https://doi.org/10.1007/s00223-020-00777-1
2. Ketteler M, Block GA, Evenepoel P *et al*. Executive summary of the 2017 KDIGO Chronic Kidney Disease–Mineral and Bone Disorder (CKD-MBD) Guideline Update: what's changed and why it matters. *Kidney Int* 2017;**92**:26–36. https://doi.org/10.1016/j.kint.2017.04.006
3. Lau WL, Obi Y, Kalantar-Zadeh K. Parathyroidectomy in the management of secondary hyperparathyroidism. *Clin J Am Soc Nephrol* 2018;**13**:952–61. https://doi.org/10.2215/CJN.10390917
4. Iorga C, Iorga CR, Andreiana I *et al*. Advantages of total parathyroidectomy in patients with secondary hyperparathyroidism induced by end stage renal disease. *Front Endocrinol* 2023;**14**:1191914. https://doi.org/10.3389/fendo.2023.1191914
5. Boudousq V, Guignard N, Gilly O *et al*. Diagnostic performance of cervical ultrasound, ^{99m}Tc-sestamibi scintigraphy, and contrast-enhanced ^{18}F-fluorocholine PET in primary hyperparathyroidism. *J Nucl Med* 2022;**63**:1081–6. https://doi.org/10.2967/jnumed.121.261900
6. Vestergaard S, Gerke O, Bay M *et al*. Head-to-head comparison of Tc-99m-sestamibi SPECT/CT and C-11-L-methionin PET/CT in parathyroid scanning before operation for primary hyperparathyroidism. *Mol Imaging Biol* 2023;**25**:720–6. https://doi.org/10.1007/s11307-023-01808-7
7. Blanco-Saiz I, Goñi-Gironés E, Ribelles-Segura MJ *et al*. Preoperative parathyroid localization. Relevance of MIBI SPECT-CT in adverse scenarios. *Endocrinol Diabetes Nutr (Engl Ed)* 2023;**70**:35–44.
8. Ishii S, Sugawara S, Yaginuma Y *et al*. Causes of false negatives in technetium-99 m methoxyisobutylisonitrile scintigraphy for hyperparathyroidism: influence of size and cysts in parathyroid lesions. *Ann Nucl Med* 2020;**34**:892–8. https://doi.org/10.1007/s12149-020-01520-4
9. Christie AC. The parathyroid oxyphil cells. *J Clin Pathol* 1967;**20**:591–602. https://doi.org/10.1136/jcp.20.4.591
10. Li S, Mao J, Wang M *et al*. Comparative proteomic analysis of chief and oxyphil cell nodules in refractory uremic hyperparathyroidism by iTRAQ coupled LC-MS/MS. *J Proteomics* 2018;**179**:42–52. https://doi.org/10.1016/j.jprot.2018.02.029
11. KDIGO. KDIGO 2017 Clinical Practice Guideline Update for the Diagnosis, Evaluation, Prevention, and Treatment of Chronic Kidney Disease—Mineral and Bone Disorder (CKD-MBD). *Kidney Int Suppl* 2017;**7**:1–59. https://doi.org/10.1016/j.kisu.2017.04.001
12. Carpentier A, Jeannotte S, Verreault J *et al*. Preoperative localization of parathyroid lesions in hyperparathyroidism: relationship between technetium-99m-MIBI uptake and oxyphil cell content. *J Nucl Med* 1998;**39**:1441–4.
13. Fagerland MW, Lydersen S, Laake P. The McNemar test for binary matched-pairs data: mid-p and asymptotic are better than exact conditional. *BMC Med Res Methodol* 2013;**13**:91. https://doi.org/10.1186/1471-2288-13-91
14. Fuster D, Torregrosa JV, Domenech B *et al*. Dual-phase 99mTc-MIBI scintigraphy to assess calcimimetic effect in patients on haemodialysis with secondary hyperparathyroidism. *Nucl Med Commun* 2009;**30**:890–4. https://doi.org/10.1097/MNM.0b013e3283305df6
15. Iwen KA, Kußmann J, Fendrich V *et al*. Accuracy of parathyroid adenoma localization by preoperative ultrasound and sestamibi in 1089 patients with primary hyperparathyroidism. *World j. surg* 2022;**46**:2197–205. https://doi.org/10.1007/s00268-022-06593-y
16. Sandrock D, Merino MJ, Norton JA *et al*. Ultrastructural histology correlates with results of thallium-201/technetium-99m parathyroid subtraction scintigraphy. *J Nucl Med* 1993;**34**:24–29.
17. Chiu ML, Kronauge JF, Piwnica-Worms, D.Effect of mitochondrial and plasma membrane potentials on accumulation of hexakis (2-methoxyisobutylisonitrile) technetium(I) in cultured mouse fibroblasts. *J Nucl Med* 1990;**31**:1646–53.
18. Hunter VR, Pauly DF, Wolkowicz PE *et al*. Mitochondrial adenosine triphosphatase in the oxyphil cells of a renal oncocytoma. *Hum Pathol* 1990;**21**:437–42. https://doi.org/10.1016/0046-8177(90)90207-L
19. Li J, Yang X, Chang X *et al*. A retrospective study of ultrasonography in the investigation of primary hyperparathyroidism: a new perspective for ultrasound echogenicity features of parathyroid nodules. *Endocr Pract* 2021;**27**:1004–10. https://doi.org/10.1016/j.eprac.2021.05.010

20. de la H, Rodríguez Á, de Nova JLM *et al*. Oxyphil cells in primary hyperparathyroidism: a clinicopathological study. *Hormones* 2021;**20**:715–21. https://doi.org/10.1007/s42000-021-00305-2
21. Mao J, You H, Wang M *et al*. Integrated transcriptomic and proteomic analyses for the characterization of parathyroid oxyphil cells in uremic patients. *Amino Acids* 2022;**54**:749–63. https://doi.org/10.1007/s00726-022-03126-8
22. Mao J, You H, Wang M *et al*. Single-cell RNA sequencing reveals transdifferentiation of parathyroid chief cells into oxyphil cells in patients with uremic secondary hyperparathyroidism. *Kidney Int* 2024;**105**:562–81. https://doi.org/10.1016/j.kint.2023.11.027
23. Berger MG, Pandian TK, Lyden ML *et al*. Preoperative imaging in renal transplant patients with tertiary hyperparathyroidism. *World J Surg* 2021;**45**:2454–62. https://doi.org/10.1007/s00268-021-06098-0
24. Whitman J, Allen IE, Bergsland EK *et al*. Assessment and comparison of ^{18}F-fluorocholine PET and ^{99m}Tc-sestamibi scans in identifying parathyroid adenomas: a metaanalysis. *J Nucl Med* 2021;**62**:1285–91. https://doi.org/10.2967/jnumed.120.257303
25. Chen YH, Chen HT, Lee MC *et al*. Preoperative F-18 fluorocholine PET/CT for the detection of hyperfunctioning parathyroid glands in patients with secondary or tertiary hyperparathyroidism: comparison with Tc-99m sestamibi scan and neck ultrasound. *Ann Nucl Med* 2020;**34**:527–37. https://doi.org/10.1007/s12149-020-01479-2
26. Aphale R, Damle N, Chumber S *et al*. Impact of fluoro-choline PET/CT in reduction in failed parathyroid localization in primary hyperparathyroidism. *World J Surg* 2023;**47**:1231–7. https://doi.org/10.1007/s00268-022-06866-6
27. Huynh KA, MacFarlane J, Newman C *et al*. Diagnostic utility of ^{11}C-methionine PET/CT in primary hyperparathyroidism in a UK cohort: a single-centre experience and literature review. *Clin Endocrinol (Oxf)* 2023;**99**:233–45. https://doi.org/10.1111/cen.14933

Received: 13.9.2024; Editorial decision: 31.1.2025